Computers and Mathematics with Applications 61 (2011) 3585–3592

Contents lists available at ScienceDirect

Computers and Mathematics with Applications

journal homepage: www.elsevier.com/locate/camwa

Lattice Boltzmann modeling of dendritic growth in forced and natural convection

D.K. Sun [a], M.F. Zhu [a,*], S.Y. Pan [a], C.R. Yang [a], D. Raabe [b]

[a] Jiangsu Key Laboratory for Advanced Metallic Materials, Southeast University, Jiangning District, Nanjing, 211189, PR China

[b] Dept. Microstructure Physics and Metal Forming, Max-Planck-Institut für Eisenforschung GmbH, Max-Planck-Str.1, D-40237 Düsseldorf, Germany

ARTICLE INFO

Keywords:
Lattice Boltzmann method
Microstructure modeling
Dendritic growth
Melt convection

ABSTRACT

A two-dimensional (2D) coupled model is developed for the simulation of dendritic growth during alloy solidification in the presence of forced and natural convection. Instead of conventional continuum-based Navier–Stokes (NS) solvers, the present model adopts a kinetic-based lattice Boltzmann method (LBM), which describes flow dynamics by the evolution of distribution functions of moving pseudo-particles, for the numerical computations of flow dynamics as well as thermal and solutal transport. The dendritic growth is modeled using a solutal equilibrium approach previously proposed by Zhu and Stefanescu (ZS), in which the evolution of the solid/liquid interface is driven by the difference between the local equilibrium composition and the local actual liquid composition. The local equilibrium composition is calculated from the local temperature and curvature. The local temperature and actual liquid composition, controlled by both diffusion and convection, are obtained by solving the LB equations using the lattice Bhatnagar–Gross–Krook (LBGK) scheme. Detailed model validation is performed by comparing the simulations with analytical predictions, which demonstrates the quantitative capability of the proposed model. Furthermore, the convective dendritic growth features predicted by the present model are compared with those obtained from the Zhu–Stefanescu and Navier–Stokes (ZS–NS) model, in which the fluid flow is calculated using an NS solver. It is found that the evolution of the solid fraction of dendritic growth calculated by both models coincides well. However, the present model has the significant advantages of numerical stability and computational efficiency for the simulation of dendritic growth with melt convection.

1. Introduction

In most solidification processes, some degree of fluid motion is nearly always present, caused either by natural buoyancy or forced convection. It is known that fluid flow might significantly perturb solute and temperature distributions, which dominates the evolution of solidification microstructures. Over the last decade, numerical studies on the interaction between melt convection and dendritic growth in pure materials and alloys have been performed based on the methods of phase field [1,2], level set [3], or cellular automata [4], usually coupled to the solution of the Navier–Stokes (NS) equations. Since the NS solvers are mean-field continuum-based approaches, it is not straightforward to properly handle the discontinuous flow velocity at the moving solid/liquid (SL) interface. The fluid flow calculation may be difficult to converge as the dendritic morphology becomes complicated with increasing solid fraction.

* Corresponding author.
E-mail address: zhumf@seu.edu.cn (M.F. Zhu).

0898-1221/$ – see front matter © 2010 Elsevier Ltd. All rights reserved.
doi:10.1016/j.camwa.2010.11.001

During the past two decades, the lattice Boltzmann method (LBM) has developed rapidly as a new and powerful tool for the numerical calculation of fluid flow, heat transport and solute transport. Compared to the conventional computational fluid dynamics, LBM has the particular merits of higher computational efficiency and better numerical stability for simulating complex fluid systems, such as multi-phase and multi-component flow phenomena under complicated geometrical boundary conditions. LBM is a kinetic-based approach that considers flows to be composed of a collection of pseudo-particles represented by a distribution function [5–8]. In this approach, the viscous fluid flow evolves automatically from the intrinsic particle streaming and collision processes by simulating the interaction of a limited number of particles [5]. Since LBM describes fluid motion at the level of the distribution functions, it can be incorporated naturally with the related simulation techniques for crystal growth in a fluid flow. Miller et al. [9] and Medvedev et al. [10] introduced phase field (PF) based models into the framework of LBM for the simulation of convective dendritic growth in a pure substance where the driving force for the phase transformation is thermal undercooling. However, few studies have been reported about applying LBM to simulate the dendritic growth in the presence of melt flow during alloy solidification. Recently, the present authors developed LBM-based models for the simulation of solutal dendritic growth of alloys in the presence of forced convection [11,12]. The models adopt LBM for numerically solving both forced fluid flow and solute transport. The kinetics of dendritic growth is determined by using a local interface composition equilibrium approach [11], or by the Gibbs–Thomson equation [12], respectively.

In this work the previously proposed LBM-based model [11] is extended to include heat transport and natural flow for the simulation of dendritic growth during alloy solidification, under consideration of forced and natural melt convection. In the proposed model, LBM is used to simultaneously calculate the melt flow, solutal transport, and thermal transport. The kinetics of the solid–liquid (SL) interface evolution is determined by the approach previously proposed by Zhu and Stefanescu (ZS) [13], which allows the accurate simulation of dendritic growth from the initial unstable stage to the steady-state stage without the requirement to include an additional kinetic parameter. We present the model details, validations through the comparison of the simulations to analytical predictions, and simulated single and multi-equiaxed dendrites.

2. Model description and numerical algorithm

In the present work, convective dendritic growth of binary alloys is considered to take place in the low Péclet number and low Reynolds number regime. The driving force for dendritic growth is determined according to the difference between the local equilibrium composition, calculated from the local temperature and curvature, and the local actual liquid composition. The local temperature and actual liquid composition are obtained by solving the thermal and solutal transport using LBM. The governing equations and numerical algorithms for calculating fluid flow, solute and temperature fields, interface curvature, crystallographic anisotropy and growth kinetics are described below.

2.1. Lattice Boltzmann method for calculating fluid flow, solutal transport, and thermal transport

In the present work, the LBM is adopted for numerically calculating fluid flow by solving the discrete Boltzmann equation on a lattice. According to the BGK approximation, the lattice Boltzmann equation (LBE), with consideration of a force term, can be expressed as [5,14]:

$$f_i\left(\boldsymbol{x}+\boldsymbol{e}_i\Delta t,\ t+\Delta t\right)-f_i(\boldsymbol{x},t)=-\left[f_i(\boldsymbol{x},t)-f_i^{\mathrm{eq}}(\boldsymbol{x},t)\right]/\tau+F_i(\boldsymbol{x},t) \tag{1}$$

where $f_i(\boldsymbol{x},t)$ is the particle distribution function (PDF) representing the probability of finding a particle at location, $\boldsymbol{x}$, at time, t, $\boldsymbol{e}_i$ is the discrete moving velocity of the pseudo-particle, Δt is the time step, τ is the relaxation time, $f_i^{\mathrm{eq}}(\boldsymbol{x},t)$ is the equilibrium PDF (EPDF), and $F_i(\boldsymbol{x},t)$ is the force term caused by the internal interaction or external fields.

LBM can also be used to simulate solute and thermal transport due to convection and diffusion. Similar to the LBE for fluid flow, the LBEs for solute and thermal transport with PDFs, $g_i(\boldsymbol{x},t)$, $h_i(\boldsymbol{x},t)$, and source terms, $G_i(\boldsymbol{x},t)$, $H_i(\boldsymbol{x},t)$, can be written as [8]:

$$g_i\left(\boldsymbol{x}+\boldsymbol{e}_i\Delta t,\ t+\Delta t\right)-g_i(\boldsymbol{x},t)=-\left[g_i(\boldsymbol{x},t)-g_i^{\mathrm{eq}}(\boldsymbol{x},t)\right]/\tau_D+G_i(\boldsymbol{x},t) \tag{2}$$

$$h_i\left(\boldsymbol{x}+\boldsymbol{e}_i\Delta t,\ t+\Delta t\right)-h_i(\boldsymbol{x},t)=-\left[h_i(\boldsymbol{x},t)-h_i^{\mathrm{eq}}(\boldsymbol{x},t)\right]/\tau_\alpha+H_i(\boldsymbol{x},t) \tag{3}$$

where τ_D, τ_α, and $g_i^{\mathrm{eq}}(\boldsymbol{x},t)$, $h_i^{\mathrm{eq}}(\boldsymbol{x},t)$ are the relaxation times and the EPDFs for solutal and thermal transport, respectively. The source terms, $G_i(\boldsymbol{x},t)$, $H_i(\boldsymbol{x},t)$, in Eqs. (2) and (3) denote the rejected solute content and the released latent heat during dendritic growth.

A widely used 2D nine-velocity (D2Q9) scheme [5] is employed in the present work, in which the space is discretized into a square lattice including nine discrete velocities, $\boldsymbol{e}_i$, given as

$$\boldsymbol{e}_i=\begin{cases}(0,\ 0), & i=0,\\ (\cos\theta_i,\ \sin\theta_i)c, \quad \theta_i=(i-1)\pi/2, & i=1,2,3,4,\\ \sqrt{2}(\cos\theta_i,\ \sin\theta_i)c, \quad \theta_i=(i-5)\pi/2+\pi/4, & i=5,6,7,8\end{cases} \tag{4}$$

where $c = \Delta x/\Delta t$ is the lattice speed, Δx is the lattice spacing. The macroscopic variables such as fluid density, ρ, velocity, $\boldsymbol{u}$, composition, C_l, and temperature, T, can be calculated from the relevant PDFs, respectively:

$$\rho = \sum_i f_i, \qquad \rho \boldsymbol{u} = \sum_i f_i \boldsymbol{e}_i + \boldsymbol{F}\Delta t/2, \qquad C_l = \sum_i g_i, \qquad T = \sum_i h_i \tag{5}$$

where $\boldsymbol{F}$ is the buoyancy force. According to the Boussinesq assumption, the buoyancy force can be expressed as

$$\boldsymbol{F} = -\boldsymbol{g}\rho_0\beta_T(T - T_0) - \boldsymbol{g}\rho_0\beta_C(C_l - C_0) \tag{6}$$

where ρ_0 is the fluid density at temperature T_0 and composition C_0, $\boldsymbol{g}$ is the gravitation acceleration, and β_C and β_T are the expansion coefficients for composition and temperature. The force term in Eq. (1) can be expressed as [14]

$$F_i(\boldsymbol{x}, t) = \left(1 - \frac{1}{2\tau}\right) w_i \left[3\frac{\boldsymbol{e}_i - \boldsymbol{u}}{c^2} + 9\frac{\boldsymbol{e}_i \cdot \boldsymbol{u}}{c^4}\boldsymbol{e}_i\right] \cdot \boldsymbol{F}\Delta t \tag{7}$$

where w_i are the weight coefficients given by $w_0 = 4/9$, $w_{1-4} = 1/9$ and $w_{5-8} = 1/36$. In the D2Q9 scheme of LBM, the EPDFs in Eqs. (1)–(3) are defined as

$$f_i^{\mathrm{eq}}(\mathbf{x}, t) = w_i\rho\left[1 + 3(\boldsymbol{e}_i \cdot \boldsymbol{u})/c^2 + 4.5(\boldsymbol{e}_i \cdot \boldsymbol{u})^2/c^4 - 1.5\boldsymbol{u}^2/c^2\right] \tag{8}$$

$$g_i^{\mathrm{eq}}(\boldsymbol{x}, t) = w_i C\left[1 + 3(\boldsymbol{e}_i \cdot \boldsymbol{u})/c^2 + 4.5(\boldsymbol{e}_i \cdot \boldsymbol{u})^2/c^4 - 1.5\boldsymbol{u}^2/c^2\right] \tag{9}$$

$$h_i^{\mathrm{eq}}(\boldsymbol{x}, t) = w_i T\left[1 + 3(\boldsymbol{e}_i \cdot \boldsymbol{u})/c^2 + 4.5(\boldsymbol{e}_i \cdot \boldsymbol{u})^2/c^4 - 1.5\boldsymbol{u}^2/c^2\right]. \tag{10}$$

According to the Chapman–Enskog analysis, the kinematic viscosity, ν, solutal diffusivity, D, and thermal diffusivity, α, are related to the relaxation times, τ, τ_D, and τ_α, respectively:

$$\nu = c^2\Delta t(\tau - 1/2)/3, \qquad D = c^2\Delta t(\tau_D - 1/2)/3, \qquad \alpha = c^2\Delta t(\tau_\alpha - 1/2)/3. \tag{11}$$

To calculate the unknown particle distribution functions at the boundary nodes of a 2D domain $\{(x, y)|0 \le x \le L, 0 \le y \le L\}$, the following boundary conditions are adopted. For the case of forced convection, the undercooled melt flows into the domain from the left-hand surface with a uniform inlet velocity $\boldsymbol{u}(x, y)|_{x=0} = (U_{\mathrm{in}}, 0)$ and flows out from the right-hand wall with $\partial_x u_x|_{x=L} = 0$. The non-equilibrium extrapolation scheme [15] is used to treat the inlet and outlet boundaries, whereas the periodic boundary conditions are imposed on the top and bottom walls. For the case of natural convection, four surfaces of the domain are treated as solid walls by imposing the bounce-back rule. The temperature at the boundary is fixed at T_0. Since there is no convection in the solid and the solute diffusion in the solid is neglected, the bounce-back scheme is applied at the SL interface for both fluid flow and solutal field calculation. The zero-flux boundary condition of $\partial_x C|_{x=0,L} = 0$ and $\partial_y C|_{y=0,L} = 0$ for solutal transfer is implemented on the four surfaces of the calculation domain.

2.2. Solution of the phase fraction evolution

As described previously, the driving force for dendritic growth is considered to be controlled by the difference between the local interface equilibrium composition and the local actual liquid composition. According to the thermodynamic concept of local equilibrium between liquid and solid phases, the interface equilibrium composition, C_l^*, can be calculated by

$$C_l^* = C_0 + \left\{T_l^* - T_l^{\mathrm{eq}} + \Gamma K\left[1 - 15\varepsilon\cos 4(\theta - \theta_0)\right]\right\}/m \tag{12}$$

where T_l^* is the interface temperature, T_l^{eq} is the equilibrium liquidus temperature at the initial composition, C_0, ε is the degree of anisotropy of the surface tension, m is the liquidus slope of phase diagram, Γ is the Gibbs–Thomson coefficient, K is the curvature of the SL interface, θ is the growth angle between the normal to the interface and the x-axis, and θ_0 is the angle of the preferential growth direction with respect to the x-axis. By solving Eqs. (1)–(3), (5), (6) and (11) within the LBM framework, the interface temperature, T_l^*, in Eq. (12) and the local actual liquid composition, C_l, can be obtained. Then, the local interface equilibrium composition, C_l^*, calculated by Eq. (12) is compared to the local actual liquid composition, C_l. If the difference satisfies $\Delta C = C_l^* - C_l > 0$ in an interface cell, the solid fraction will increase. According to the solute equilibrium condition at the interface, during one time step interval, Δt, the increased solid fraction, $\Delta\phi_s$, of an interface cell can be evaluated by $\Delta\phi_s = (C_l^* - C_l)/[C_l^*(1 - k)]$, where k is the solute partition coefficient. As solid fraction increases, solute is rejected at the SL interface. Solute partition between liquid and solid at the SL interface is considered according to $C_s = kC_l$. The released solute and latent heat in an interface cell at each time step can be evaluated as $\Delta C_l = \Delta\phi_s C_l(1 - k)$ and $\Delta T = \Delta\phi_s\Delta H/C_p$, respectively. Here, ΔH is the volumetric latent heat and C_p is the specific heat. Thus, the source terms in Eqs. (2) and (3) can be calculated with $G_i(\boldsymbol{x}, t) = w_i\Delta\phi_s C_l(1-k)$ and $H_i(\boldsymbol{x}, t) = w_i\Delta\phi_s\Delta H/C_p$. If the cell is fully solidified, the rejected solute amount, $w_i\Delta\phi_s C_l(1-k)$, is added to the solute distribution function of its surrounding neighbor interface or liquid cells. When the sum of the solid fraction in an interface cell equals one, the state of this cell is assigned as solid and its surrounding liquid cells are explicitly captured as the new interface cells. However, the exact SL front is implicitly

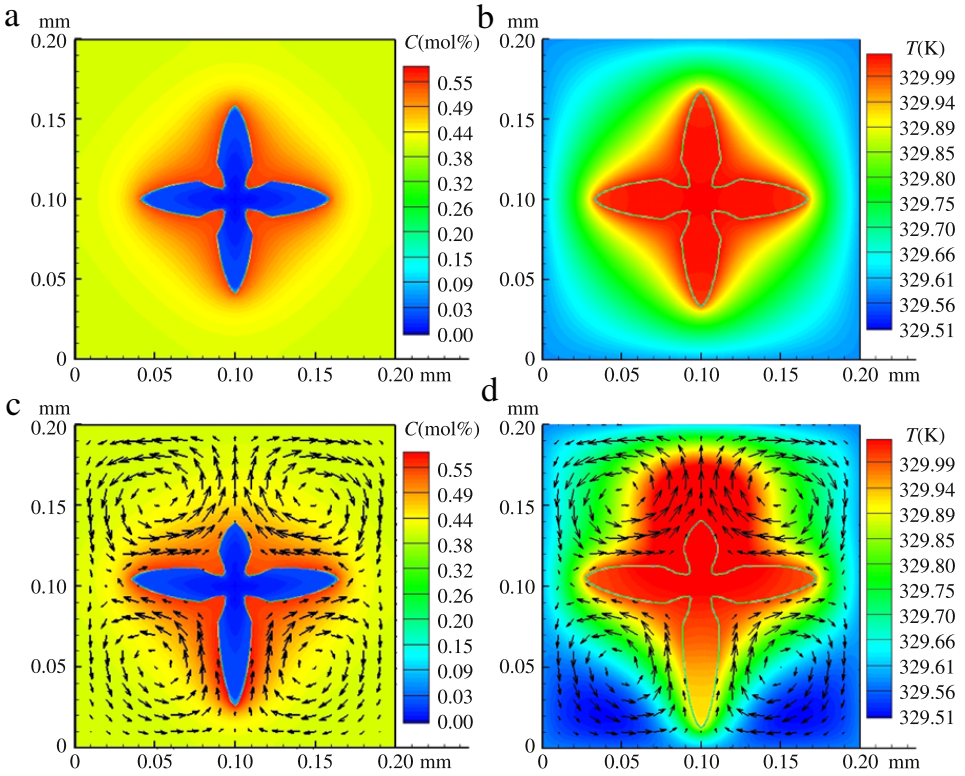

Fig. 1. Simulated morphologies of a dendrite freely growing in an undercooled melt ($\Delta T = 0.8$ K) without convection ((a) and (b), the growth time is 1.0845 s) and with natural convection ((c) and (d), the growth time is 0.7768 s) for a binary alloy ($C_0 = 0.4$ mol%). Here, (a) and (c) show the solutal field, and (b) and (d) show the thermal field, for $F_s = 0.09$. The velocity vector plots indicate the strength and direction of natural flow (F_s: global solid volume fraction in the domain).

scaled by the solid fraction within each interface cell. The local interface curvature, K, and the growth angle, θ, are calculated according to the solid fraction gradient at the SL interface with the equations:

$$K = \left[2\partial_x\phi_s\partial_y\phi_s\partial^2_{xy}\phi_s - (\partial_x\phi_s)^2\partial^2_y\phi_s - (\partial_y\phi_s)^2\partial^2_x\phi_s\right] \cdot \left[(\partial_x\phi_s)^2 + (\partial_y\phi_s)^2\right]^{-3/2} \tag{13}$$

$$\theta = \arccos \partial_x\phi_s \left[(\partial_x\phi_s)^2 + (\partial_y\phi_s)^2\right]^{-1/2}. \tag{14}$$

The present model can simulate dendritic morphology with various preferential crystallographic orientations. However, since the trapping rule for new interface cells is based on a cellular automaton (CA) approach, and the interface curvature is calculated by the partial derivatives of solid fraction with respect to the x- and y-axes (Eq. (13)), which might yield different curvature values along the different directions, the present model for simulating dendritic growth still reveals some artificial anisotropy of the CA square mesh.

3. Results and discussion

3.1. Dendritic growth in conjunction with natural convection

Natural buoyancy convection resulting from the density difference due to the thermal and the solutal gradient can be characterized by the dimensionless thermal Rayleigh number $\mathrm{Ra}_T \equiv g\beta_T \Delta T_{\mathrm{Ra}} L^3/(\nu\alpha)$ and the composition Rayleigh number $\mathrm{Ra}_C \equiv g\beta_C \Delta C_{\mathrm{Ra}} L^3/(\nu D)$, where $\Delta T_{\mathrm{Ra}} = T_t^* - T_0$ is the difference between the steady-state upstream tip temperature and initial temperature, $\Delta C_{\mathrm{Ra}} = C_t^* - C_0$ is the difference between the steady-state upstream tip concentration and initial concentration, and L is the domain length. Simulations were performed to study the effects of natural buoyancy on the free dendritic growth in an undercooled melt. The calculation domain consists of 400×400 meshes with a mesh size of 0.5μm. Fig. 1 presents the simulated morphologies of a single dendrite freely growing in an undercooled melt of $\Delta T = 0.8$ K without convection (Fig. 1 (a) and (b)) and with natural convection (Fig. 1 (c) and (d)) for a binary alloy with $C_0 = 0.4$ mol%. The parameters used for these simulations are as follows: $k = 0.1$, $m = -2.3$ K/(mol%), $\Gamma = 6.9 \times 10^{-8}$ m K, $\varepsilon = 0.0267$, $\Delta H = 5 \times 10^3$ J/m^3, $C_p = 1940$ J/(m$^3 \cdot$ K), $\nu = 6.0 \times 10^{-9}$ m^2/s, $D = 1.0 \times 10^{-9}$ m^2/s, $\alpha = 3.0 \times 10^{-9}$ m^2/s. In the case of natural convection, the Rayleigh numbers are taken as $\mathrm{Ra}_C = \mathrm{Ra}_T = 5 \times 10^3$. The relaxation time for fluid flow calculation, LBM time step, and dendritic growth time step are taken as $\tau = 2.0$, $\Delta t_1 = 2.083 \times 10^{-5}$ s, and $\Delta t_2 = 6.249 \times 10^{-5}$ s, respectively. It can be seen from Fig. 1 (a) and (b) that in a purely diffusive environment the symmetrical composition field, temperature field, and dendritic morphology can be obtained. Since the thermal diffusivity is larger than the solutal

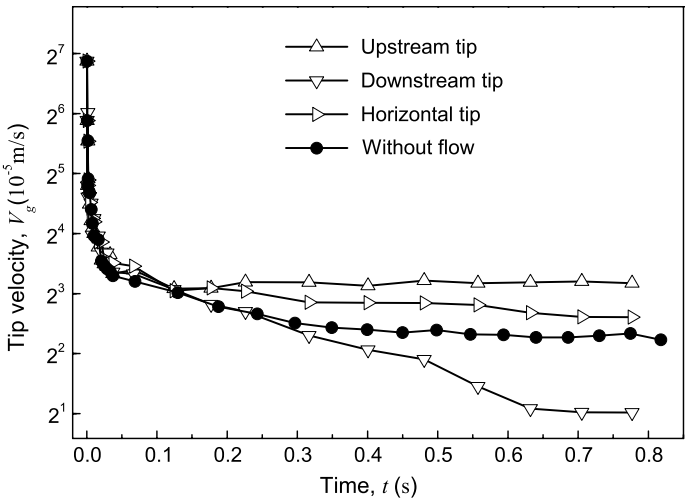

Fig. 2. Tip velocities versus time for the cases of Fig. 1.

diffusivity, the thermal diffusion layer is wider than the solute diffusion layer. On the other hand, when the buoyancy effect caused by gravity is considered, the buoyancy convection carries the solute and heat released at the interface away from the upstream (lower) region to the downstream (upper) region, resulting in the asymmetrical composition and temperature fields. According to Eq. (12), the lower the interface temperature, T_l^*, the higher the interface equilibrium composition, C_l^*, will be. Together with a reduced actual composition, C_l, at the interface of the upstream tip, the difference of $\Delta C = C_l^* - C_l$ in the upstream tip will be larger than that in the downstream tip, leading to a higher growth velocity of the upstream tip compared to the downstream tip. The upstream arm is thus rapidly developed, whereas the growth of the downstream arm is retarded. Fig. 2 indicates the evolution of the tip velocities corresponding to the cases of Fig. 1. As shown, all tip velocities start from a large value and decrease rapidly. After a transient period, the velocities of different tips reach approximately stable values with different levels. The steady-state velocities of the upstream and downstream tips are higher and lower than that without flow, respectively. Moreover, the downstream tip needs a longer time to approach the steady state. The horizontal tip has an intermediate tip velocity that is close to the one without convection.

To validate the present model, we derived the modified 2D thermal and solutal Ivantsov solutions, including the effects of convection according to the method given in Ref. [16], and they are given by

$$\Omega_T = \sqrt{\pi P_T}\exp(P_T)\left[\operatorname{erfc}\left(\sqrt{P_T}\right) - \operatorname{erfc}\left(\sqrt{P_T\,(1+2\delta_T/R)}\right)\right] \tag{15}$$

$$\Omega_C = \sqrt{\pi P_C}\exp(P_C)\left[\operatorname{erfc}\left(\sqrt{P_C}\right) - \operatorname{erfc}\left(\sqrt{P_C\,(1+2\delta_C/R)}\right)\right] \tag{16}$$

where Ω_T is the dimensionless thermal undercooling, Ω_C is the dimensionless solutal supersaturation, $P_T \equiv VR/(2\alpha)$ and $P_C \equiv VR/(2D)$ are the thermal and solutal Péclet numbers, and V and R are the tip velocity and radius. δ_T and δ_C are the thickness of the thermal and solutal layers, which can be computed as

$$\frac{\delta_C}{R} = \lambda \mathrm{Ra}_C^{-1/4}\left(1 + \frac{\sqrt{\mathrm{Le}}}{N}\right)^{-1/4} \tag{17}$$

$$\frac{\delta_T}{R} = \lambda \mathrm{Ra}_T^{-1/4}\left(1 + \frac{N}{\sqrt{\mathrm{Le}}}\right)^{-1/4} \tag{18}$$

where Le is the Lewis number (Le $\equiv \alpha/D$). The coefficient λ is chosen to be 2.2 [17]. The buoyancy number N can be obtained as

$$N = \frac{\beta_C(C_t^* - C_0)}{\beta_T(T_t^* - T_0)} \tag{19}$$

where C_t^* and T_t^* are the concentration and the temperature in the liquid at the dendritic tip. Substituting the modified Ivantsov solutions into the 2D Lipton–Glicksman–Kurz (LGK) model, according to the method proposed in Ref. [17], the analytical predictions of the steady-state velocity and radius of the upstream tip in the presence of natural convection can be obtained. To solve the modified LGK model, the selection parameter, σ^*, is determined according to the linearized solvability theory [18] that considers σ^* as a function of the anisotropy parameter, ε. For $\varepsilon = 0.0267$, used in this work, the corresponding value of σ^* by the linearized solvability model is 0.1065. Table 1 presents a comparison between simulations and analytic results for the steady-state velocities and radii of the upstream tip at various initial compositions in the presence of natural convection with the Rayleigh numbers $\mathrm{Ra}_T = \mathrm{Ra}_C = 5.0\times 10^3$. The tip radii are obtained using a parabolic fit to the

Table 1
Comparison between simulations and analytical predictions for the steady-state velocities and radii, and the simulated selection parameters, σ^*, of the upstream tip at various initial compositions ($\Delta T = 0.8$ K, $\mathrm{Ra}_T = \mathrm{Ra}_C = 5.0 \times 10^3$).

C_0 (mol%)	Velocity (10^{-5} m/s)		Radius (10^{-6} m)		σ^*
	Theory	Simulation	Theory	Simulation	Simulation
0.4	8.923	9.004	2.144	1.795	0.1415
0.5	7.954	6.857	2.117	1.750	0.1717
0.6	7.179	5.783	2.096	1.667	0.1997
0.7	6.545	5.283	2.081	1.654	0.1983

simulated dendritic shape as described in Ref. [13]. The values of the selection parameter, σ^*, calculated from the simulated tip velocities and radii according to the LGK definition, are also given in Table 1. It is noted that the simulated tip velocities and radii are mostly slightly lower than the theoretical data. Nevertheless, the agreement between the simulations and the analytical predictions appears to be reasonable. The selection parameter, σ^*, calculated from the simulations, is found to be larger than the theoretical value of 0.1065, due to both lower tip velocity and radius obtained from the simulations. In addition, the simulated σ^* is not a constant, but varies with the initial composition. The quantitative phase field simulations performed by Ramirez and Beckermann also found a breakdown of the LGK selection criterion [19].

3.2. Dendritic growth in conjunction with forced convection

In the present work, for the simulation of dendritic growth with forced convection, the buoyancy effect is ignored and thus the force term in Eq. (1), $F_i(\boldsymbol{x}, t)$, is taken to be zero. The forced flow is generated by imposing a uniform inlet flow velocity provided as U_{in} at the left-hand boundary. In addition, for the sake of simplicity, the thermal transport is not considered and the temperature field inside the domain is considered to be uniform.

The model validation for dendritic growth with forced convection was performed by comparing the simulations with the Oseen–Ivantsov solution [20], which establishes a relationship among the growth Péclet number $P_C \equiv VR/(2D)$, the flow Péclet number $P_f \equiv UR/(2D)$, and the driving force for growth (V: tip velocity, R: tip radius, U: flow velocity, D: solute diffusivity). For the composition-driven dendritic growth of alloys during isothermal solidification, the driving force is considered to be the dimensionless solutal supersaturation, Ω_C. The Oseen–Ivantsov solution can then be expressed as

$$\Omega_C = P_C \exp\left(P_C - P_f\right) \int_1^{\infty} \exp\left\{-P_C\eta + P_f\left[2 + \int_1^{\eta} \mathrm{g}\left(\zeta\right)\zeta^{-1/2}\mathrm{d}\zeta - \eta\right]\right\} \eta^{-1/2}\mathrm{d}\eta. \tag{20}$$

The function $\mathrm{g}(\zeta)$ in Eq. (20) is defined as

$$\mathrm{g}(\zeta) = \frac{\sqrt{\zeta}\,\mathrm{erfc}\left(\sqrt{\mathrm{Re}\zeta/2}\right) + \sqrt{2/(\pi\mathrm{Re})}\left[\exp(-\mathrm{Re}/2) - \exp(-\mathrm{Re}\zeta/2)\right]}{\mathrm{erfc}\left(\sqrt{(\mathrm{Re}/2)}\right)} \tag{21}$$

where $\mathrm{Re} \equiv UR/\nu$ is the Reynolds number. Considering that the Oseen–Ivantsov solution was originally derived based on the convective dendritic growth in a pure substance, where only thermal transport is calculated, and that the thermal diffusion is a two sided problem, we adopted an equal solid/liquid solutal diffusivity, i.e., $D_s = D_l$, for this particular simulation. The simulations were performed for an Al-4.5 wt% Cu alloy with various inlet flow velocities and a constant melt undercooling of $\Delta T = 6.80$ K in a rectangle domain $\{(x, y)|0 \le x \le L/2, 0 \le y \le L\}$, where $L = 80\ \mu m$. The lattice space was taken as $\Delta x = 0.2\ \mu m$. The simulated steady-state tip equilibrium composition, C_l^*/C_0, equals 1.506. The dimensionless supersaturation can be calculated as $\Omega_C = (C_l^* - C_0)/[C_l^*(1-k)] = 0.405$. The steady-state velocity and radius of the upstream tip, with various inlet flow velocities, were simulated and measured as described in Refs. [11,12]. The simulated growth Péclet number and flow Péclet number can then be calculated with $P_C = VR/(2D_l)$ and $P_f = U_{\mathrm{in}}R/(2D_l)$, respectively. The comparison between the simulation and the analytical solution is given in Fig. 3. As shown, the simulated data of P_C versus P_f are very close to the profile of the Oseen–Ivantsov solution.

The present model was also applied to simulate the multi-dendritic growth behavior. Fig. 4 shows the simulated multi-dendritic morphology of an Al-3.0 wt% Cu alloy. The figures on the upper row depict the pure diffusive dendrites and the lower ones the convective dendrites growing from a forced flowing melt with an inlet flow velocity of $U_{\mathrm{in}} = 0.001$m/s. The calculation domain was divided into 400×400 elements, each with a mesh size of 1.0μm. Initially, six seeds with randomly preferred orientations were placed on the domain. The melt temperature was assumed to be uniform and cooled down from the liquidus with a cooling rate of 10 K/s. Fig. 4 shows that fluid flow also plays a notable role in the growth of multi-dendrites, particularly at the early stage of solidification. Melt flows, from left to right, smoothly along the small dendrites, during which solute is transported from the upstream side to the downstream side of each dendrite. Asymmetric dendritic features are thus produced. As the dendrites grow close to each other, the flow gradually fades away in the inter-dendrite region.

To further examine the potential of the present model, a comparison is made between the present model and the ZS–NS model, where the fluid flow is calculated using an NS solver. Fig. 5 presents the evolution of solid fraction calculated from two models under the conditions of Fig. 4. As shown, two curves coincide well before the solid fraction is about $F_s = 0.25$.

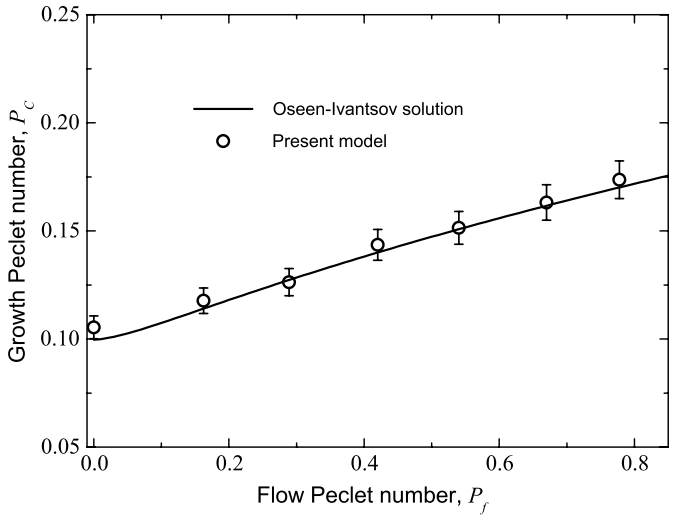

Fig. 3. The growth Péclet number as a function of the flow Péclet number ($\Omega_C = 0.405$).

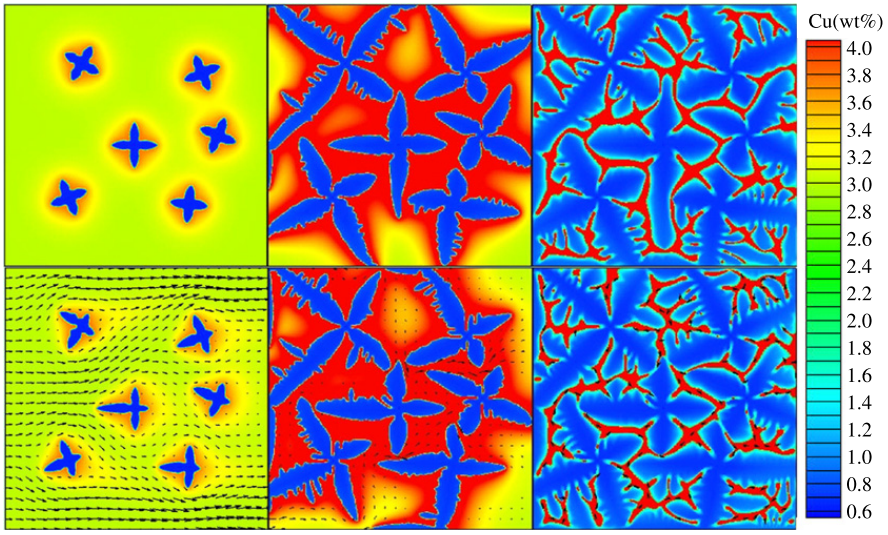

Fig. 4. Evolution of multi-dendritic morphology without flow (upper row) and with a flow velocity of $U_{\text{in}} = 0.001$ m/s (bottom row); $F_s = 0.05$, 0.35 and 0.85, from left to right.

Since the flow calculation did not converge when using the NS solver, the ZS–NS simulation could not be performed when the solid fraction was above about 0.25. However, the present model can model the multi-dendritic growth until the solid fraction reaches about 0.97. Moreover, the calculation time of the present model is about 40 min with $F_s = 0.25$ (PC Core 2 Duo, CPU-2.67 GHz), which is about twelve times faster than that achieved with the ZS–NS model. Accordingly, it is apparent that the present model has the significant merits of being computationally efficient and numerically stable for the simulation of complex phase transformation problems during solidification in the presence of melt convection.

4. Conclusions

An LBM-based model is presented to model the dendritic growth of alloys with natural and forced convection. Instead of continuum-based NS solvers, the kinetic-based LBM is used to numerically solve the coupled flow, solute, and temperature fields. Based on the LBM calculated solutal and thermal fields, the evolution of the SL interface is determined according to a local solute equilibrium approach. The model validations were performed by comparing simulations to analytical predictions. The simulated upstream tip velocities and radii of the dendrite growing in a melt with natural convection are found to agree reasonably with the predictions of the modified LGK model that accounts for the effects of convection. For the convective dendritic growth in a forced flow, the simulated growth Péclet number of the upstream tip, as a function of the flow Péclet number, is very close to the Oseen–Ivantsov solution. The simulation results of single and multi-dendritic growth of binary alloys with natural and forced convection illustrate the nature of interaction among melt flow, solute and thermal transport, and phase transition. The comparison with the ZS–NS model indicates that the present model is numerically

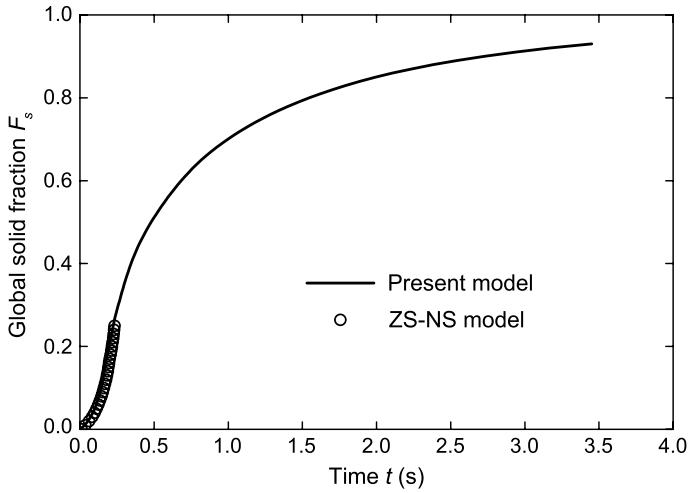

Fig. 5. Comparison of the evolution of solid fraction calculated by the present model and the ZS–NS model.

more stable and computationally more efficient, as well as simpler to be implemented for the simulation of phase transition problems incorporated with melt convection.

Acknowledgements

The authors wish to thank Professor Doru M. Stefanescu at the Ohio State University for the helpful discussion, and Dr. Bruce W. Krakauer at AO Smith Corporate Technology Center for the modification in English. This work was supported by NSFC (Grant Nos. 50671025 and 50971042) and RFDP of China (Grant No. 20070286021).

References

[1] X. Tong, C. Beckermann, A. Karma, Q. Li, Phase-field simulations of dendritic crystal growth in a forced flow, Phys. Rev. E 63 (2001) 061601.
[2] C.W. Lan, C.J. Shih, Efficient phase field simulation of a binary dendritic growth in a forced flow, Phys. Rev. E 69 (2004) 031601.
[3] L. Tan, N. Zabaras, A level set simulation of dendritic solidification with combined features of front-tracking and fixed-domain methods, J. Comput. Phys. 211 (2006) 36–63.
[4] M.F. Zhu, S.Y. Lee, C.P. Hong, Modified cellular automaton model for the prediction of dendritic growth with melt convection, Phys. Rev. E 69 (2004) 061610.
[5] Y.H. Qian, D. d'Humières, P. Lallemand, Lattice BGK models for Navier–Stokes equation, Europhys. Lett. 17 (1992) 479–484.
[6] D. Raabe, Overview of the lattice Boltzmann method for nano- and microscale fluid dynamics in materials science and engineering, Modelling Simul. Mater. Sci. Eng. 12 (2004) R13–R46.
[7] L.-S. Luo, Theory of the lattice Boltzmann method: lattice Boltzmann models for nonideal gases, Phys. Rev. E 62 (2000) 4982–4996.
[8] B. Deng, B.C. Shi, G.C. Wang, A new lattice Bhatnagar–Gross–Krook model for the convection–diffusion equation with a source term, Chin. Phys. Lett. 22 (2005) 267–270.
[9] W. Miller, I. Rasin, F. Pimentel, Growth kinetics and melt convection, J. Cryst. Growth 266 (2004) 283–288.
[10] D. Medvedev, T. Fischaleck, K. Kassner, Influence of external flows on pattern growth, J. Cryst. Growth 303 (2007) 69–73.
[11] D. Sun, M. Zhu, S. Pan, D. Raabe, Lattice Boltzmann modeling of dendritic growth in a forced melt convection, Acta Mater. 23 (2009) 1755–1767.
[12] D. Sun, M. Zhu, S. Pan, D. Raabe, Numerical modeling of dendritic growth in alloy solidification with forced convection, Int. J. Mod. Phys. B 57 (2009) 1609–1614.
[13] M.F. Zhu, D.M. Stefanescu, Virtual front tracking model for the quantitative modeling of dendritic growth in solidification of alloys, Acta Mater. 55 (2007) 1741–1755.
[14] Z.L. Guo, C.G. Zheng, B.C. Shi, Discrete lattice effects on the forcing term in the lattice Boltzmann method, Phys. Rev. E 65 (2002) 046308.
[15] Z.L. Guo, C.G. Zheng, B.C. Shi, Non-equilibrium extrapolation method for velocity and pressure boundary conditions in the lattice Boltzmann method, Chin. Phys. 11 (2002) 366–374.
[16] B. Cantor, A. Vogel, Dendritic solidification and fluid flow, J. Cryst. Growth 44 (1977) 109–123.
[17] Q. Li, C. Beckermann, Modeling of free dendritic growth of succinonitrile-acetone alloys with thermosolutal melt convection, J. Cryst. Growth 236 (2002) 482–498.
[18] A. Barbieri, J.S. Langer, Predictions of dendritic growth rates in the linearized solvability theory, Phys. Rev. A 39 (1989) 5314–5325.
[19] J.C. Ramirez, C. Beckermann, Examination of binary alloy free dendritic growth theories with a phase-field model, Acta Mater. 53 (2005) 1721–1736.
[20] P. Bouissou, P. Pelce, Effect of a forced flow on dendritic growth, Phys. Rev. A 40 (1989) 6673–6680.